Testbed for extended-scene Shack-Hartmann and phase retrieval wavefront sensing

Rhonda M. Morgan*, Catherine M. Ohara, Joseph J. Green, Jennifer Roberts, Erkin Sidick, Kirill V. Shcheglov
Jet Propulsion Laboratory, 4800 Oak Grove Drive, Pasadena, CA, USA 91109

DRAFT

ABSTRACT

We have implemented a testbed to demonstrate wavefront sensing and control on an extended scene using Shack-Hartmann and MGS phase retrieval simultaneously. This dual approach allows for both high sensitivity and high dynamic range wavefront sensing. Aberrations are introduced by a silicon-membrane deformable mirror. The detailed characterization of this mirror and its sensitivity matrix are presented. The various Shack-Hartmann algorithms, including a maximum likelihood approach are discussed and compared to phase retrieval results using a point source. The next phase of the testbed will include results with extended scenes.

Keywords: Wavefront sensing, Shack-Hartmann, phase diversity, extended scene, deformable mirror, active optics

1. INTRODUCTION

Phase Retrieval wavefront sensing can achieve high resolution wavefront measurements (1), while Shack-Hartmann wavefront sensing offers high dynamic range. Both techniques could be employed in a hand-off scenario to provide both high resolution and high dynamic range. We have implemented a testbed that performs simultaneous Phase Retrieval and Shack-Hartmann wavefront sensing. A small deformable mirror allows for control of the wavefront and the introduction of known aberrations.

The wavefront sensing and control is proven first with a point source. A known aberration is introduced, measured, and iteratively controlled using the Shack-Hartmann Camera. The initial state and the flattened stated are measured by the Phase Retrieval Camera for verification. The goal of the testbed is to repeat this cycle using an extended scene as the source.

Phase Retrieval uses defocused images acquired on both sides of focus to calculate the phase of the wavefront in the exit pupil of the system. The algorithm used in the testbed is a Modfied Girchberger-Saxton(1). A Shack-Hartmann sensor employs an array of lenslets at a pupil. Each subaperture is imaged to a point, the displacement of the point image, or centroid offset is measured. The centroid offset is used to calculate the tilt in the wavefront over the subaperture. The Shack-Hartmann measures the derivative of the wavefront.

2. TESTBED HARDWARE

The testbed employs a deformable mirror (DM) to introduce a known aberration that is measured by both a Shack-Hartmann Camera (SHC) and a Phase Retrieval Camera (PRC). The Phase Retrieval Camera was used to measure JWST prototype mirrors and is described in detail elsewhere(1). The DM is characterized in the following section. The main component of the testbed is a field projector consisting of three identical off-axis parabolas (OAPs). The field projector provides a pupil to both the PRC and SHC that is conjugate to the DM. The source is a mercury-zenon arclamp delivered through a liquid light guide, and imaged through a diffuser onto the target. The targets contained in the filter wheel include a 15 um pinhole, a 25 um pinhole, a fine bar target, a coarse bar target, and a coarse grid. The target is located at the focus of an OAP. The OAP collimates the light beam. The collimated beam is incident on the DM then reimaged through two matched OAPs to the exit pupil. A beamsplitter diverts one beam to the entrance pupil of the PRC and allows the main beam to continue to the Shack-Hartmann lenslet array.

*rhonda.m.morgan@jpl.nasa.gov

The lenslet array has pitch 300 um and f/25.3, on 5 micron pixels which results in 8 pixels per Airy disc. The sensitivity was expected to be 0.0015 waves and 287 waves dynamic range. The spatial sampling of the DM is nearly 7 subapertures per 2 mm actuator spacing.

The field magnification is the focal length of the lenslet/focal length of the OAP, which is a ratio of 12.5 The field stop is 4.76 mm for 100% fill. The target resolution for 1 pix = 72 um and for 1 airy disc = 833 um.5

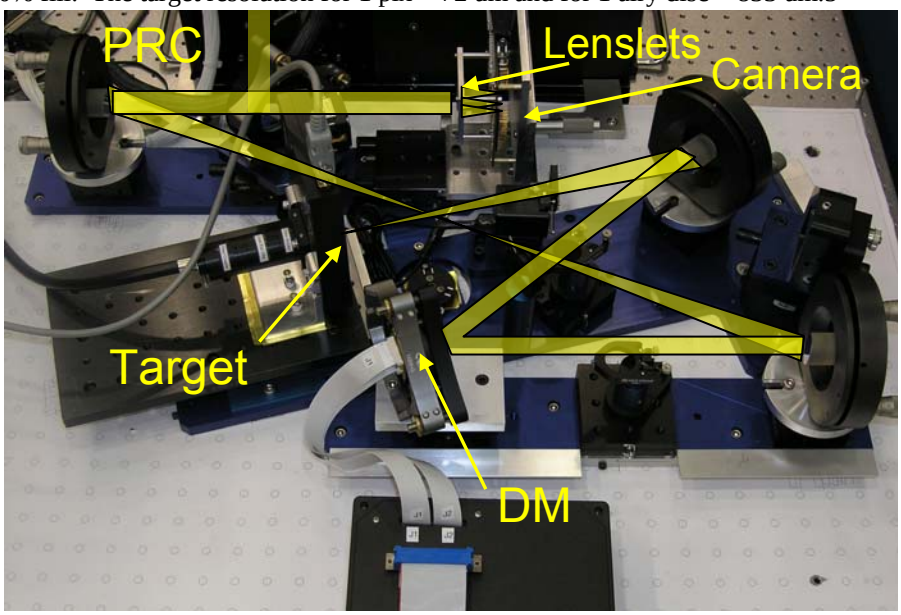

Figure 1: The field projector relays the DM surface to the entrance pupil of the PRC and to the Shack-Harmann lenslet array.

2.1. Deformable Mirror

The deformable mirror (DM) is an electrostatic device consisting of a thin silicon membrane mirror surface, a gap, and a plate of 37 pads. A voltage applied to one of the pads creates an electric field that pulls on the membrane. The mirror was developed and supplied by Agiloptics (formerly Intellite) and initial characterization is presented in (2). The mirror is 16 mm diameter. The flatness of the DM when powered off was measured on a Zygo to be about 1.4 waves peak-to-valley, largely astigmatism. Maximum deflection is a focus mode, peak to valley of 6 microns. A single influence function varies in height, from 160 nm to 200 nm PV. The influence functions do not provide enough dynamic range to create a flat wavefront. All the measurements, sensing and control, were performed in a relative mode.

The membrane displacement is proportional to the applied voltage squared. The linearity with V2 was tested. At low voltages, the results are noisy, and varied from actuator to actuator. The behavior is not exactly linear in V2 and was fit with a polynomial second order in V. The fit is compared to measured displacements for three actuators in Figure XX. The variation from actuator to actuator is about 10%. The sensitivity matrix was built based on an average, knowing that there would be a 10% variation. We plan to build a second generation matrix that incorporates the nonlinearities of each individual actuator.

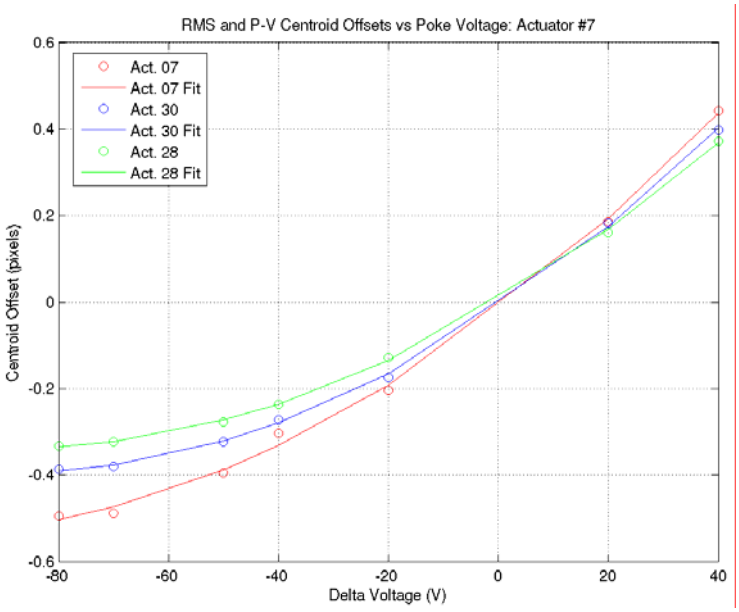

The sensitivity matrix used in the control of the DM is composed from the vectors of centroid position for each DM actuator at maximum safe voltage. The sensitivity matrix includes the second-order fit to the voltage.

$$\vec{\mathbf{c}}_{xy} = \begin{bmatrix} \vec{\mathbf{c}}_x \\ \vec{\mathbf{c}}_y \end{bmatrix} : \text{Centroid position vector [2Mx1]}$$

$$\tilde{\mathbf{C}}_{xy} = \left[\vec{\mathbf{c}}_{xy1} \;\; \vec{\mathbf{c}}_{xy2} \ldots \vec{\mathbf{c}}_{xyN}\right] : \text{Centroid position matrix [2MxN]}$$

$$\Delta V = V - V_{\text{nom}} : V_{\text{nom}} \quad \text{is the reference bias}$$

$$\Delta s_o = \left[\sqrt{\left(\vec{\mathbf{c}}_x - \vec{\mathbf{c}}_{xnom}\right)^2 + \left(\vec{\mathbf{c}}_y - \vec{\mathbf{c}}_{ynom}\right)^2}\right]_{P-V} = a\Delta V^2 + b\Delta V + c,\; V = 140V,\; V_{\text{nom}} = 100V$$

$$\tilde{\mathbf{S}}_{\text{c}} = \frac{\tilde{\mathbf{C}}_{xy} - \tilde{\mathbf{C}}_{\text{nom}}}{\Delta s_o} = \frac{\Delta\tilde{\mathbf{C}}_{xy}}{\Delta s_o} : \text{Centroid offset sensitivity matrix [2MxN]}$$

$$\tilde{\mathbf{G}}_{\text{c}} = \tilde{\mathbf{S}}_{\text{c}}^{+} : \text{ [2MxN] Gain Matrix (Pseudo - inverse of } \tilde{\mathbf{S}}_{\text{c}})$$

$$\Delta\vec{\mathbf{s}} = \begin{bmatrix} \Delta s(V_1) \\ \Delta s(V_2) \\ \\ \Delta s(V_N) \end{bmatrix} : \text{ [Nx1] vector corresponding to the voltages of N - actuators}$$

$$\Delta\vec{\mathbf{c}}_{xy} = \tilde{\mathbf{S}}_c \Delta\vec{\mathbf{s}} \qquad (1)$$

$$\Delta\vec{\mathbf{s}} = \tilde{\mathbf{G}}_c \Delta\vec{\mathbf{c}}_{xy} \qquad (2)$$

$$\Delta\vec{\mathbf{v}} = \frac{-b + \sqrt{b^2 - 4a(c - \Delta\vec{\mathbf{s}})}}{2a} \qquad (3)$$

3. SHACK-HARTMANN ALGORITHMS

Centroiding algorithms were initially developed and optimized for the ground based astronomical observing challenges of low signal and fast changing atmospheres. Traditional centroiding algorithms are center of mass calculations based on a quad cell and the noise is dependent on ratio of PSF to cell size(3). This testbed uses a focal plane array with 8 pixels per Airy disc, strong signal, a quasi-static environment and longer times for computing. This allowed other regions of the solution space of centroiding algorithms to be explored in the hopes of yielding greater accuracy.

We developed two algorithms, center of mass with FFT-based PSF centering (CC) and a Maximum Likelihood Gaussian fit to the PSF (MLG) and baselined them to a traditional iterative center of mass (COM) in a circular window. The algorithms were compared under three tests: windowing, shot noise, and bias.

3.1. Rms centroiding error vs. integration time

The rms error testing was performed on synthetic SH 20x20 PSF spot images. The PSF's were allowed to vary randomly in a 5x5 pixel area. 400 results (one image) were averaged for each datapoint. All noise was modeled as added white gaussian noise. Only shot noise, dark current shot noise, and readout noise were included.
The following parameters were used: readout noise of 40 e/pix, dark current of 125 e/sec/pix, and total flux in terms of counts/sec/PSF (flux through one lenslet). A single PSF is the Fourier transform of a hexagonal aperture and has a Gaussian width (radius of the 1/e point) of 1.72 pixels.

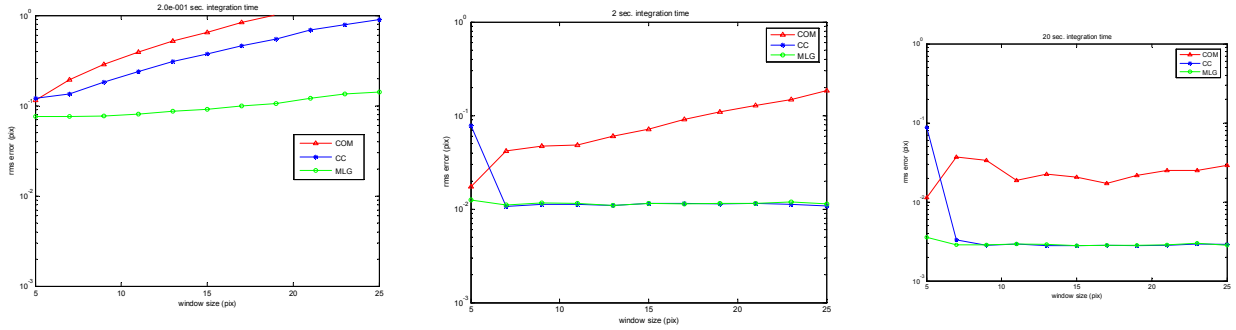

Figure X. Centroid error for integration times of 0.2 sec, 2 sec, and 20 sec.

3.2. Window Tests

The window tests are mainly relevant for the COM algorithm. The simulations were performed assuming a 33000 counts/sec/PSF incident flux. For the COM algorithm, a 5 pixel window seems to be ideal for all integration times for this PSF. The other two algorithms were fairly insensitive to the window size for a reasonably large window.

3.3. Shot Noise Tests

The shot noise limit is calculated in a continuous approximation for a Gaussian spot that best matches the central PSF.

$$\frac{d\left(\frac{1}{\sigma_x^2}\right)}{dA} = \frac{\left(\frac{\partial I(x,y)}{\partial x}\right)^2}{I(x,y)+N^2} \qquad \frac{1}{\sigma_x^2} = \iint \frac{\left(\frac{\partial I(x,y)}{\partial x}\right)^2}{I(x,y)+N^2} dxdy \qquad (5)$$

Where I(x,y) is the psf intensity and N is the portion of the noise that is constant for each pixel (i.e., readout noise and dark current shot noise). Assuming N=0 and a gaussian PSF.

$$I(x,y) = Ae^{-\frac{(x^2+y^2)}{w^2}}$$

we obtain $\sigma_x = \sigma_y = \frac{1}{\sqrt{2\pi A}}$ and $\sigma_r = \frac{1}{\sqrt{\pi A}}$

In the following tests centroiding error was calculates for different incident photon flux conditions and different integration times. A shot noise limit is shown for comparison.

Figure X. The rms centroid error as a function of integration time for various flux levels.

One noteworthy difference between MLG/CC algorithms and COM algorithm is the plateau exhibited by the COM algorithm at long integration times. That error seems to be due to centroiding bias and can in principle be compensated out.

3.4. Bias Tests

The three algorithms were tested for bias using an over-sampled pixel (5x5 point array centered at the pixel center) assuming a 100% fill factor. The (1,1) position corresponds to the pixel center. Row and Column coordinates are in 1/20th of a pixel (the whole image is one pixel)

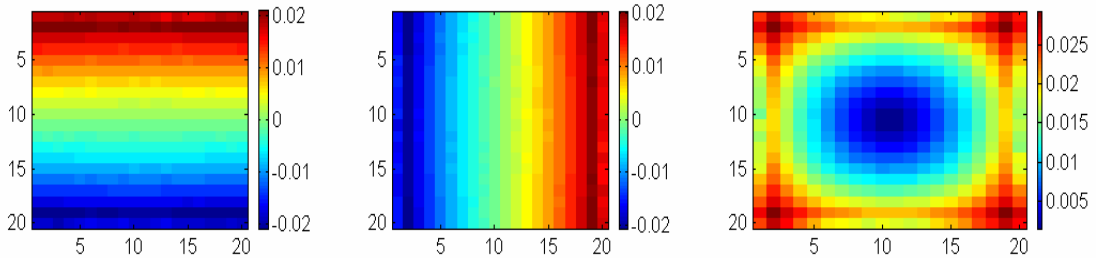

Center of Mass: Row, Column, r

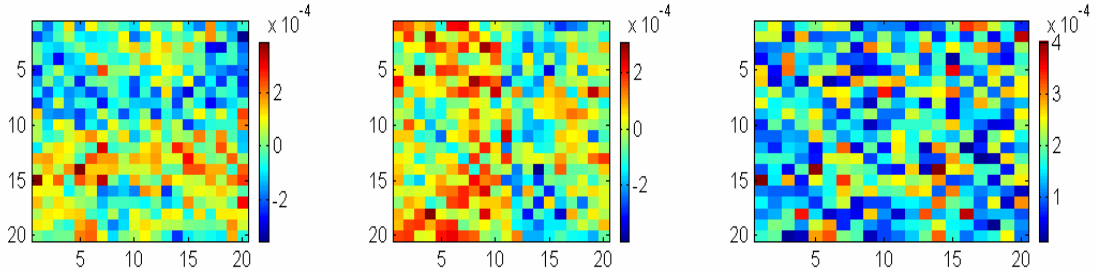

Center of Mass with FFT centering

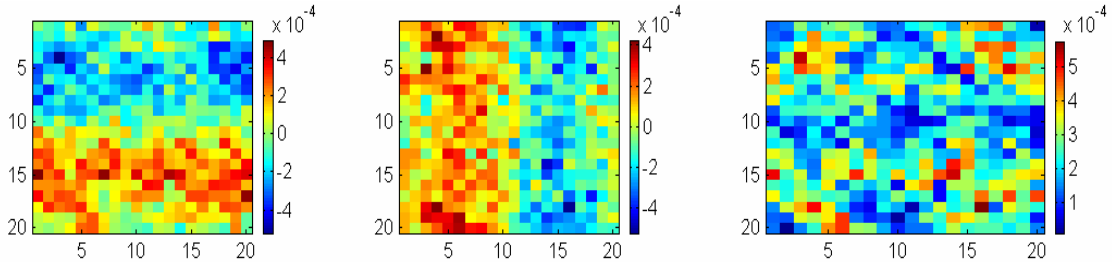

Maximum Likelihood Gaussian

Figure X: The bias within the centroiding window is only a factor for the center of mass (COM) algorithm.

3.5. Algorithms Summary

The straight COM algorithm is the fastest and has reasonable performance. However, it's sensitive to the choice of the window size. The window size can be tunes to maximize performance for a given PSF shape and noise parameters. Also, it has a built-in systematic error which is periodic in sub-pixel centroid position. This error depends on the exact PSF shape and can be significant (systematic errors as large as 0.03 pixels were observed for the simulated hexagonal PSF). This error is the result of the granularity in choosing the window bounds (the CC algorithm which shifts the PSF does not suffer from this problem). For very broad PSF's and good SNR's the COM performance comes very close to the ML algorithm performance, so the gain from the extra computation is marginal (less than 50% improvement in accuracy).

The MLG algorithm does a 2-D quadratic weighted least-squares fit to the PSF position probability distribution. It is almost as fast as the COM algorithm, however it requires an approximate centroid as a starting point, so it is best thought of as an add-on on top of a COM algorithm. Another limitation is that the PSF must be substantially Gaussian-like and of reasonable (a few pixels) width. It is not appropriate for very tight PSF's, such as in a quad-nulling scheme.

The iterative centroiding with FFT-based PSF centering (CC) algorithm is by far the slowest, however it has very good performance at high SNR's and is insensitive to the shape of the PSF. For low SNR's is not the best choice.

Given a priori knowledge of the PSF shape, an MLG algorithm can be devised that will combine fast calculation speed and performance at the theoretical noise limit.

4. POINT-SOURCE PERFORMANCE

4.1. Wavefront control with the Shack-Hartmann

Using a point source, the influence functions were measured, the sensitivity matrix built and the wavefront controlled. A known aberration of random pokes was applied to the DM and measured with the SHC. The wavefront error was 58 nm rms and 345 nm PV. Three iterations of the control scheme were applied. The wavefront error was controlled to 6 nm rms, 54 nm P-V. Some of the actuators were saturated. The control could be improved by implementing individual actuator nonlinearities.

Before Control: Random Actuator Pokes

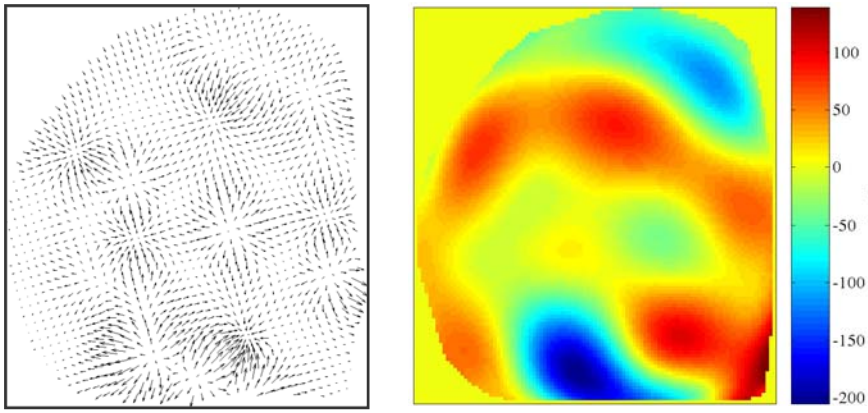

RMS = 58nm, PV = 345nm

After 3 iterations of SH Sensing & Control

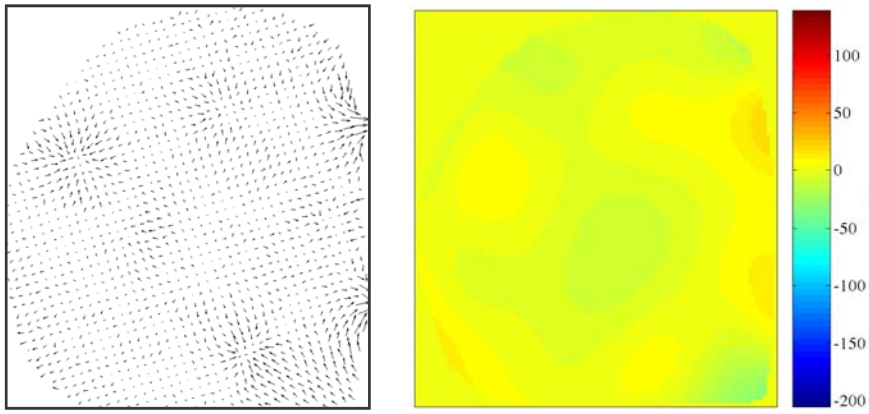

RMS = 6nm, PV = 54nm

4.2. Comparison of Phase Retrieval to Shack-Hartmann

The wavefronts measured by the PRC and the SHC must be registered, or co-aligned. This is difficult without fiducials. The individual actuator influence functions are used as fiducials. The certainty is limited by the certainty in an individual wavefront measurement. After translating and scaling, the wavefronts are compared, shown in Figure X. The wavefront as measured by the PRC and the SHC are subtracted leaving a 5 nm rms residual. This residual provides for superb hand-off between the two instruments. The residual is below the accuracy of the SHC measurements.

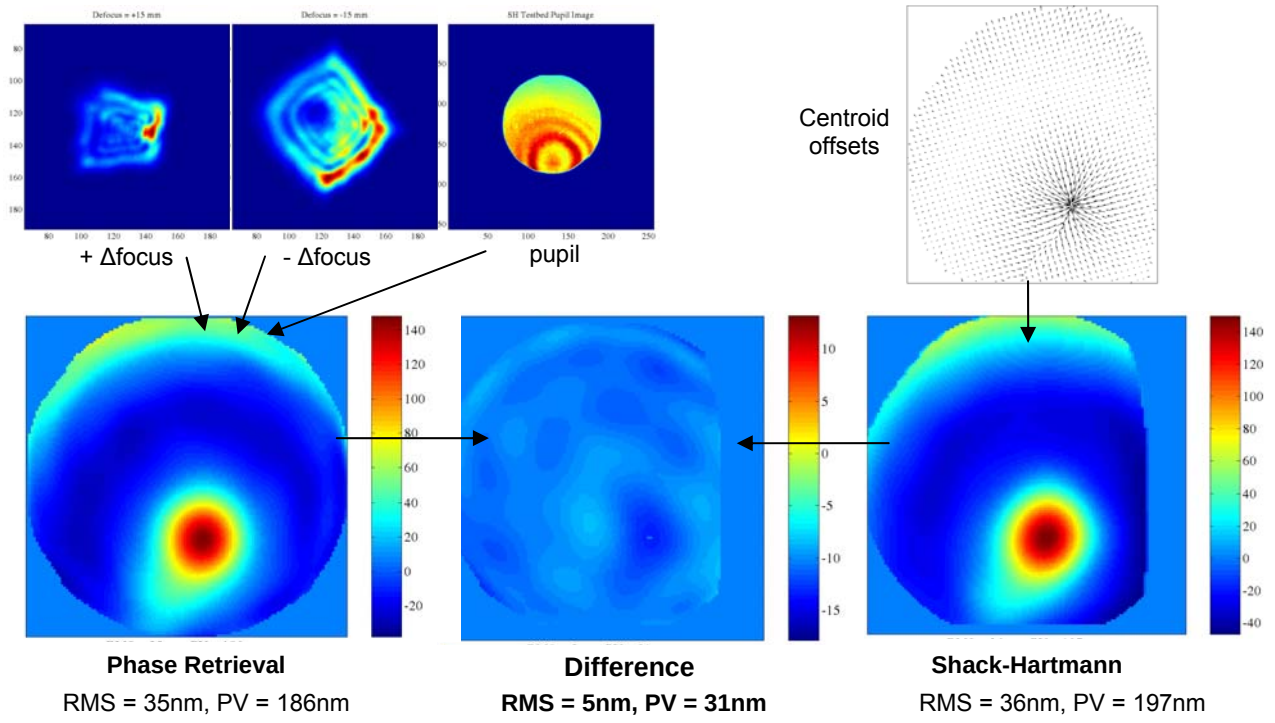

5. EXTENDED-SCENE PRELIMINARY RESULTS

The ultimate goal of the testbed is to perform the above wavefront control utilizing an extended scene. An extended scene appears on the SHC as an array of small images (subimages). A field stop is necessary to constrain the subimages within the centroid window and to prevent subimage overlap. The centroid position of each subimage is determined by correlation. These correlation algorithms are currently in development. The preliminary hardware results we present in Figure X are examples of extended scene Shack-Hartmann images. The small bar target is scene through the PRC, which has a much larger field of view and a finer resolving power, than the SHC.

Shack-Hartmann

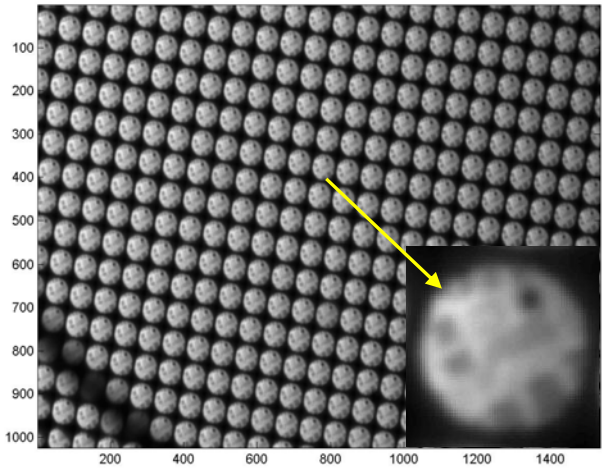

Phase Retrieval Camera

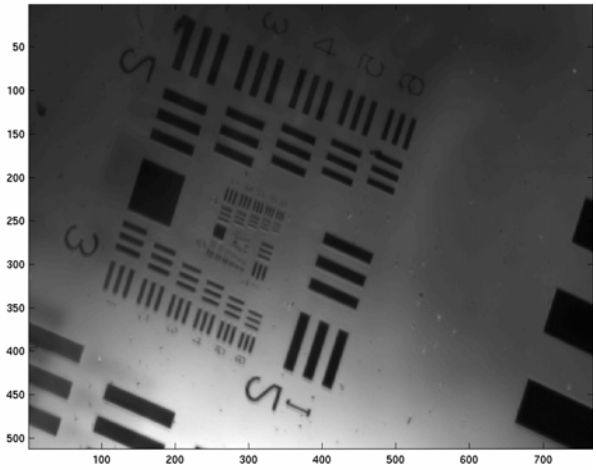

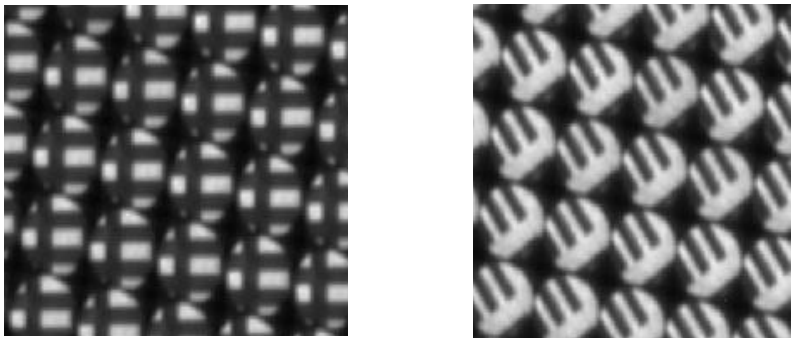

Figure X: Extended scene targets as scene by the Shack-Hartmann and the PRC (upper right).

6. CONCLUSIONS

We have implemented a testbed that allows simultaneous measurement of a wavefront with a Shack-Hartmann Camera and a Phase Retrieval Camera. Measurements with the two cameras agree to 5 nm rms. Aberrated wavefronts are generated by a deformable mirror that has been well characterized and can provide 6 um of focus deflection. The wavefront has been controlled to 6 nm rms using the SHC in point-source mode. The testbed is ready to enter its next phase, which is wavefront control using extended scenes.

ACKNOWLEDGEMENTS

This research was performed at the Jet Propulsion Laboratory, California Institute of Technology under contract to the National Aerospace Administration.

REFERENCES

1. Joseph J. Green, David C. Redding, Yuri Beregovski, Andrew E. Lowman, Catherine M. Ohara, "Intermerometric validation of image-based wavefront sensing for NGST," in *IR Space Telescopes and Instruments*, John C. Mather ed., Proc SPIE 4850, pp. 345-352, 2003
2. David C. Dayton, Justin D Mansell, John D Gonglewski, Sergio R. Restaino, "Characterization and Control of a novel micromachined membrane mirror for adaptive wavefront control," in *High-Resolution Wavefront Control: Methods, Devices, and Applications III*, J.D. Gonglewski, M. A. Voronstov, M.T. Gruneisen, ed., Proc SPIE **4492,** pp 29-34, 2002.
3. John H. Hardy, *Adaptive Optics for Astronomical Telescopes*, Oxford University Press, 1998